Am J Physiol Regul Integr Comp Physiol 285: R243–R254, 2003;
10.1152/ajpregu.00472.2002.

Direct interstitial infusion of NK_1-targeted neurotoxin into the spinal cord: a computational model

Malisa Sarntinoranont,[1] Michael J. Iadarola,[2] Russell R. Lonser,[3] and Paul F. Morrison[1]

[1]*Division of Bioengineering and Physical Science, Office of Research Services,* [2]*Pain and Neurosensory Mechanisms Branch, National Institute of Dental and Craniofacial Research, and* [3]*Surgical Neurology Branch, National Institute of Neurological Disorders and Stroke, National Institutes of Health, Bethesda, Maryland 20892*

Submitted 7 August 2002; accepted in final form 4 March 2003

Sarntinoranont, Malisa, Michael J. Iadarola, Russell R. Lonser, and Paul F. Morrison. Direct interstitial infusion of NK_1-targeted neurotoxin into the spinal cord: a computational model. *Am J Physiol Regul Integr Comp Physiol* 285: R243–R254, 2003; 10.1152/ajpregu.00472.2002.—Convection-enhanced delivery of substance P (SP) nocitoxins to the spinal cord interstitium is under consideration for the treatment of chronic pain. To characterize treatment protocols, a three-dimensional finite-element model of infusion into the human dorsal column was developed to predict the distribution of SP-diphtheria toxin fusion protein (SP-DT′) within normal and target tissue. The model incorporated anisotropic convective and diffusive transport through the interstitial space, hydrolysis by peptidases, and intracellular trafficking. For constant SP-DT′ infusion (0.1 μl/min), the distribution of cytotoxicity in NK_1 receptor-expressing neurons was predicted to reach an asymptotic limit at 6–8 h in the transverse direction at the level of the infusion cannula tip (~60% ablation of target neurons in lamina I/II). Computations revealed that SP-DT′ treatment was favored by a stable SP analog (half-life ~60 min), high infusate concentration (385 nM), and careful catheter placement (adjacent to target lamina I/II). Sensitivity of cytotoxic regions to NK_1 receptor density and white matter protease activity was also established. These data suggest that intraparenchymal infusions can be useful for treatment of localized chronic pain.

convection-enhanced delivery; intraparenchymal infusions; pain therapy; pharmacodynamic model; convection; finite-element method

INVESTIGATORS INTERESTED in treating persistent pain conditions have taken advantage of the substance P (SP)-mediated endocytotic pathway, using it as a transport system to deliver cytotoxic fusion proteins to neurokinin type 1 receptor (NK_1R)-expressing neurons located within the dorsal horn of the spinal cord. SP-saporin toxin, SP-diphtheria toxin (SP-DT′), and SP-*Pseudomonas* exotoxin conjugates have been identified as capable of selectively lesioning second-order spinal cord neurons, thereby blocking nociceptive transmission mediated by small-diameter Aδ and C fibers and, possibly, Aβ fibers (5, 15, 28, 35, 52). In this study, we investigate the transport and drug delivery of SP-DT′ (~47,000 mol wt), a COOH-terminal truncated diphtheria toxin that retains the transmembrane and catalytic domains of diphtheria toxin but replaces the native binding domain with SP (15) or an analog of SP [(pGlu^5,MePhe^8, MeGly^9)-substance P-(5–11) (DiMeC7)] stabilized against peptidase activity (14).

Previous animal studies investigating NK_1R-targeted neurotoxins have used intrathecal delivery to circumvent the blood-brain barrier. In the rat, intrathecal infusion of these compounds has been shown to significantly reduce hyperalgesia (5, 28). However, a major challenge remains in achieving this effect at the larger scale of primates and humans. In these species, the principal cell targets, laminae I and II of the dorsal horn, lie deeper in the spinal cord and are not in direct contact with the intrathecal cerebrospinal fluid (CSF), as in the rat. Consequently, the neurotoxins must traverse a much greater distance within the primate or human spinal cord tissue and, given the slow rate of macromolecular diffusion in tissue (43), be substantially more exposed to the degradative action of endogenous peptidases. As a result, these therapeutic molecules are unlikely to reach their target cells in sufficient concentration to be efficacious, and the need for a different mode of drug delivery is indicated. In addition, intrathecal infusion results in bilateral treatment. However, many conditions are localized, and, in such cases, a more discrete application would be therapeutically advantageous.

An alternative to intrathecal delivery is direct interstitial infusion or convection-enhanced delivery (CED) (7, 25, 32). By this method, an agent is infused directly into the nervous tissue via a cannula and is transported through the interstitial space primarily by convection, or bulk flow, allowing for greater volume transmission and control over exposure (7, 24, 25, 32). To anticipate the tissue distribution of administered agents by infusion into the central nervous system (CNS), mathematical models of CED have been developed. Early models accounted for the distribution into gray matter regions of the brain, characterized by isotropic transport and mechanical properties (3, 4, 32). More recently, a three-dimensional image-based

Address for reprint requests and other correspondence: M. Sarntinoranont, Drug Delivery and Kinetics Resource, Div. of Bioengineering and Physical Science, ORS, NIH, Bldg. 13, Rm. 3N17, 13 South Dr., Bethesda, MD 20892-5766 (E-mail: sarntinm@mail.nih.gov).

The costs of publication of this article were defrayed in part by the payment of page charges. The article must therefore be hereby marked "*advertisement*" in accordance with 18 U.S.C. Section 1734 solely to indicate this fact.

finite-element model of CED into the spinal cord has been developed (44) that captures transport in gray and anisotropic white matter regions and accounts for the distribution of albumin observed in rat spinal cord.

Interstitial transport is anisotropic within white matter (7, 41, 42) because of preferential diffusion and fluid flow in the interstitial space parallel to axonal fibers. Taking advantage of this low-resistance pathway, Lonser et al. (26) and Wood and colleagues (54) showed that direct infusion into the white matter dorsal column provides a basis for safe distribution of macromolecules over significant volumes of the spinal cord. In the present study, we extend the anisotropic CED model (44) to describe SP-DT′ transport when the toxin is infused into the white matter dorsal column of the human spinal cord. The objective of an effective chronic pain therapy is to reach nociceptive neurons located in laminae I, II, and X in concentrations adequate to induce cytotoxicity while, at the same time, avoiding the destruction of anterior motor neurons or other cells within the spinal cord that express the NK_1R (1, 6). To address these constraints, the model incorporated primary transport considerations, including regional anatomic boundaries, interstitial fluid flow, enzymatic degradation, and binding of SP-DT′ to target neurons. Ultimately, cytosolic diphtheria toxin blocks cellular protein synthesis and kills the cell. By coupling intracellular trafficking kinetics (45) to the model, cytosolic concentrations of toxin were determined which provided a basis for predicting regions of cell death.

METHODS

Spinal cord geometry. The spinal cord geometry was created from a single transverse section of the spinal cord at the C_7 level, on which white and gray matter regions, including the different lamina, were outlined (Fig. 1). Visualization and finite-element meshing programs (Amira, version 2.3, TGS, San Diego, CA; Gambit, version 1.3, Fluent, Lebanon, NH) were used to project the segmented outlines 20 mm in the craniocaudal (z) direction, creating separate white and gray matter volumes. [Craniocaudal variation in the projected area (between C_6 and C_8) was neglected. Also, greater projection lengths had no significant effect on fluid flow distribution.] A spherical infusion site (radius = 0.306 mm) was incorporated into the white matter dorsal column ($x = 0$, $y = 0$, $z = 0$). The epicenter of the site was 0.45 mm lateral to the dorsal median fissure, 2.14 mm posterior to lamina X, and 2.10 mm anterior to the external surface of the spinal cord. Reflection symmetry about the transverse plane through the infusion site was assumed. Overall dimensions of the final spinal cord geometry (Fig. 1) are as follows: craniocaudal, 20.0 mm (40.0 mm with symmetry); mediolateral, 10.9 mm; and dorsoventral, 6.54 mm. In computations examining the sensitivity of distribution to infusion site location, secondary locations were considered in which the infusion site was shifted 0.8 mm laterally toward lamina I and 1.6 mm anteriorly toward lamina X.

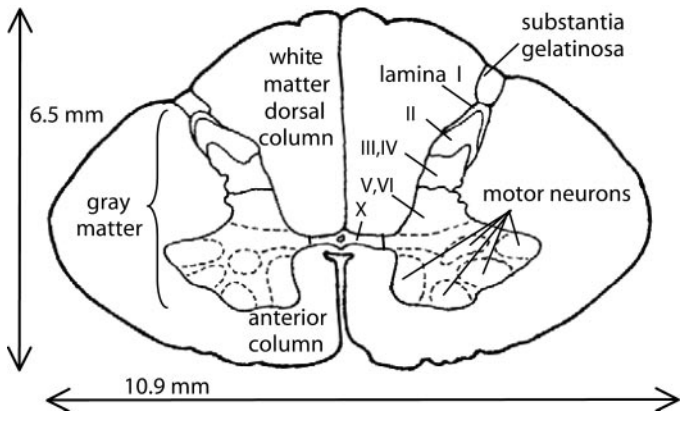

Fig. 1. Outline of gray and white matter regions of human spinal cord at the C_7 level, modified from Haines (19) with dimensions from Hausman (20).

Interstitial fluid flow. To describe fluid flow in the spinal cord, the tissue was treated as a porous medium composed of an interstitial volume phase through which bulk flow occurs and a noninterstitial "solid" phase composed of intercellular matrix, cells, white matter fibers, and blood vessels. Fluid and solute transport through porous media is described by a continuum model accounting for differential mass and momentum balances. For steady-state flow conditions, conservation of fluid mass is expressed by the continuity relation

$$\nabla \cdot \bar{u} = 0 \qquad (1)$$

where $\nabla\cdot$ is the divergence operator and $\bar{u}$ is the volume-averaged fluid velocity. The contribution of fluid sources and sinks would require the inclusion of additional pressure-dependent terms proportional to the difference in interstitial and capillary pressure. However, such terms were neglected in this model, because tissues of the CNS are devoid of an active lymphatic system (9), characterized by low rates of fluid transfer across the capillary walls at the pressures encountered during interstitial infusion at a moderate flow rate (32), subject to negligibly low rates of water formation by metabolism (22), and because only isotonic solutions of SP-DT′ were considered. The momentum equation is expressed by Darcy's law

$$\bar{u} = -\kappa \cdot \nabla p \qquad (2)$$

where κ is the hydraulic conductivity tensor, ∇ is the gradient operator, and p is the interstitial fluid pressure. κ is a measure of the conductance of the material to fluid flow and is dependent on pore geometry and the structure of the interstitial matrix. κ is isotropic in gray matter (12, 25) but highly anisotropic in white matter because of the presence of the aligned nerve fibers (7, 26). White matter hydraulic anisotropy is quantified by large values of $\kappa_{wm\text{-}z}/\kappa_{wm\text{-}x}$, which is the ratio of the hydraulic conductivity of white matter in the craniocaudal direction, parallel to the aligned fibers, to the hydraulic conductivity of white matter in the transverse direction (Table 1).

The model was limited to a description of flow through a rigid porous medium. Only low volumetric flow rates were considered, and elastic expansion effects were accounted for by increasing the interstitial volume fraction (ϕ) from the normal value of 0.20 to 0.26 (12, 40, 44). In the present study, ϕ and κ were derived from data specific for an infusion rate of 0.1 μl/min (26, 44, 54). Boundary conditions were such that a volumetric infusion rate of 0.1 μl/min was applied at the infusion site boundary, and zero fluid pressure conditions were applied at the external spinal cord-CSF boundaries. Along the symmetrical plane ($z = 0$), symmetry boundary conditions were assumed: $\bar{u}\cdot\bar{n} = 0$, where $\bar{n}$ is the unit normal vector to the surface. At the far end of the tissue ($z =$

Table 1. *Interstitial transport parameters*

	Value	Ref
$D_{wm\text{-}x}$, $D_{wm\text{-}y}$	1.34×10^{-7} cm²/s	Calculated from 41, 48
$D_{wm\text{-}z}$	2.29×10^{-7}	Calculated from 41, 48
D_{gm}	1.60×10^{-7} cm²/s	48
$\kappa_{wm\text{-}z}/\kappa_{wm\text{-}x}$	20	44
$\kappa_{wm\text{-}x}/\kappa_{gm}$	100	34
ϕ	0.26	36, 44

D, effective diffusivity; wm, white matter; gm, gray matter; ϕ, interstitial volume fraction.

20 mm), fluid pressure was approximated as zero, because the vast majority of fluid is routed into the surrounding CSF before it reaches this point. (Applying $\bar{u} = 0$ along this boundary resulted in negligible changes in the velocity profile.)

SP receptor-mediated delivery. As the SP-DT′ complex moves through the extracellular space, it is subject to protein degradation and cellular interaction. Data of Garland et al. (16), Bowden et al. (8), and Grady et al. (18) were used to develop a simple kinetic model (Fig. 2) of SP binding and intracellular trafficking (45). This kinetic model incorporates the principal trafficking steps, including surface binding between SP and NK_1R, clathrin-mediated endocytosis followed by spatial translation to a perinuclear endosome, where SP is sorted from its receptor, rapid degradation of SP once sorted to the late endosomes/early lysosomes, and return of sorted receptor to plasma membrane via recycling endosomes. In addition, the model follows previous research allowing for a very low rate of transfer of the diphtheria toxin moiety from early sorting endosomes to cytosol (57). Incorporation of this trafficking model into the present model allowed for estimation of the cytosolic diphtheria toxin concentration, which is ultimately responsible for cell kill.

Transport equations were derived by applying mass conservation to SP-DT′ and the NK_1R in their various compartments: SP_e (SP-DT′ in the extracellular space), B (bound SP-DT′ on the cell surface), R (free NK_1R on the cell surface), SP_s (early/sorting endosomal SP-DT′), R_s (NK_1R in early/sorting endosomes), R_{post} (NK_1R in recycling endosomes), and C_{cyt} (SP-DT′/diphtheria toxin in cytosol). The relation governing interstitial transport of SP_e is (all concentrations expressed on a tissue averaged basis)

$$\frac{\partial SP_e}{\partial t} = \nabla\cdot(D\nabla SP_e) - 1/\phi\nabla\cdot(\bar{u}SP_e) - k_m SP_e - k_1 SP_e R + k_2 B \quad (3)$$

where t is time and D is the effective diffusivity tensor of the interstitium and ϕ is the interstitial volume fraction. Other constants are k_m (rate of degradation by peptidases) and k_1 and k_2 (rates of SP-DT′ association and dissociation from the receptor). The first two terms on the right-hand side of *Eq. 3* correspond to diffusive and convective transport, respectively. Competitive binding with native SP was neglected because of the low endogenous levels present [~0.4 nM, calculated from measures of capsaicin-evoked release of SP-like immunoreactivity in guinea pig dorsal horn sections from Geppetti et al. (17)] compared with the high SP-DT′ concentrations considered for therapy (tissue-averaged values of 20, 100, and 200 nM) and the large pool of NK_1R available for binding (~12–23 nM). Equations associated with binding and cellular trafficking within NK_1R-expressing neurons are given by

$$\frac{dB}{dt} = k_1 SP_e R - k_2 B - k_i B \quad (4)$$

$$\frac{dSP_s}{dt} = k_i B - k_s SP_s \quad (5)$$

$$\frac{dC_{cyt}}{dt} = k_{trans} SP_s \quad (6)$$

$$\frac{dR}{dt} = -k_1 SP_e R + k_2 B + k_{rcyc} R_{post} \quad (7)$$

$$\frac{dR_s}{dt} = k_i B - k_s R_s \quad (8)$$

and

$$\frac{dR_{post}}{dt} = k_s R_s - k_{rcyc} R_{post} \quad (9)$$

Intracellular trafficking constants are as follows: k_i (rate of SP-DT′ internalization), k_{trans} (rate of SP-DT′ transfer from endosome to cytosol), k_s (rate of SP-DT′ and NK_1R intracellular sorting), and k_{rcyc} (rate of NK_1R transfer from the recycling endosomes to the cell surface). Because NK_1R are conserved

$$B_{max} = B + R + R_s + R_{post} \quad (10)$$

where B_{max} is the NK_1R capacity and varies within different laminae of the spinal cord.

To determine the temporal and spatial distribution of the SP-DT′ complex, *Eqs. 1–10* were solved over the spinal cord volume. For the initial condition before infusion, concentration of membrane-bound NK_1R (R) was set equal to the corresponding B_{max}. All other concentrations were initially zero. Concentration of SP_e at the infusion site boundary was set equal to ϕC_{inf} where ϕ is the tissue porosity and C_{inf} is the infusate concentration, a constant value (77, 385, and 770

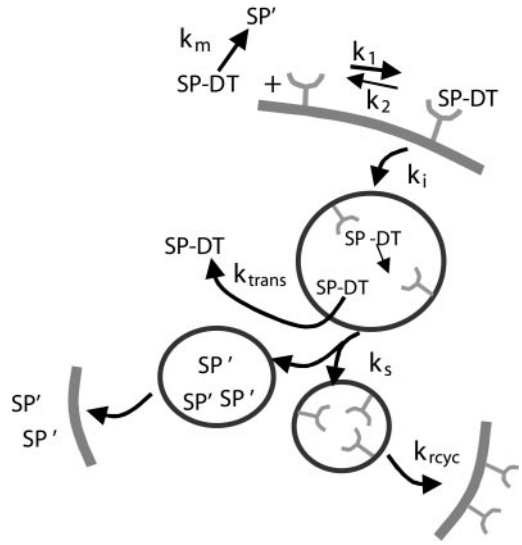

Fig. 2. Schematic of substance P (SP) trafficking model. SP′, partially degraded SP-diphtheria toxin (SP-DT′) peptide pool; k_m, rate of degradation by peptidases; k_1 and k_2, rates of association and dissociation, respectively, of the receptor; k_i, rate of SP-DT′ internalization; k_{trans}, rate of SP-DT′ transfer from endosome to cytosol; k_s, rate of SP-DT′ and neurokinin type 1 receptor (NK_1R) intracellular sorting; k_{rcyc}, rate of NK_1R transfer from recycling endosomes to cell surface.

nM). Transport of SP_e across the external spinal cord/CSF surfaces was assumed to be dominated by convection, with negligible loss due to diffusion ($-\phi D\nabla SP_e \cdot \bar{n} = 0$). Along the symmetrical plane ($z = 0$), SP_e flux normal to the surface was set to zero ($\nabla SP_e \cdot \bar{n} = 0$).

Parameter values. Parameters are tabulated in Tables 1 and 2. Tissue porosity and hydraulic conductivity values for gray and white matter were taken from a previous analysis of albumin infusion in the rat cord (44). Effective diffusivity in gray matter (D_{gm}) was taken from measures of a similar-molecular-weight protein (i.e., albumin, ~66,000 mol wt) in brain tissue (48), and the tensor components of the effective diffusivity in white matter ($D_{wm\text{-}x}$, $D_{wm\text{-}y}$, and $D_{wm\text{-}z}$) were estimated from measurements of anisotropic diffusion in the spinal cord (41). Rate constants k_1, k_2, k_i, k_s, and k_{rcyc} were taken from previous analysis (45) of the data of Garland et al. (16), Bowden et al. (8), and Grady et al. (18). The gray matter degradation rate ($k_{m\text{-}gm}$) was set equivalent to an SP half-life of 60 min (14). Some sensitivity studies were also performed using an SP gray matter half-life of 3 min. SP_e degradation rate in white matter interstitium was bracketed by setting it equal to the CSF degradation rate (23) or to one-half of the gray matter rate. The latter is a high-end estimate that accounts for the absence of enkephalinase activity in white matter (39) but allows for degradation by peptidases that have not been quantitatively characterized (11). Receptor capacities (B_{max}) ranged from zero in the white matter, where no NK_1R are detectable (13), to tissue-averaged concentration values of 23 nM, reflective of the receptor densities in laminae I, II, and X (1). Sensitivity to changes in receptor capacity was also analyzed.

Diphtheria toxin cytotoxicity analysis is dependent on the rate of transfer of toxin from the endosome to cytosol, as determined by k_{trans}. Although this parameter has not been determined specifically for SP-DT′, it is known to depend heavily on the toxic moiety and is independent of the cell line involved (57). Accordingly, the value of k_{trans} in our target neurons has been roughly approximated by the 3.5×10^{-5} min^{-1} value measured previously for diphtheria toxin conjugated to transferrin (57). (Sensitivity computations show that substantial uncertainty can be tolerated in this parameter, because the steep leading edge of the C_{cyt} profiles renders the cytotoxic contours insensitive to nearly order-of-magnitude uncertainties in the cytosolic concentrations of the diphtheria toxin moiety.)

Table 2. *SP-DT′ and NK_1 receptor parameters*

	Value	Ref
k_1	0.79 nM^{-1} min^{-1}*†	10
k_2	0.035 min^{-1}*	10, 51
k_{rcyc}	0.029 min^{-1}*	8
k_i	0.15 min^{-1}*	16
k_s	0.048 min^{-1}*	16
$k_{m\text{-}gm}$	0.0116 min^{-1}	14
$k_{m\text{-}wm}$	0.000052 min^{-1}	23
	0.00578 min^{-1}	See text
k_{trans}	0.00003 min^{-1}	57
B_{max}		
Lamina I/II	23.0 nM	1
Lamina III–IX	12.5 nM‡	1
Lamina X	21.0 nM‡	1

SP-DT′, substance P-diphtheria toxin; NK_1R, neurokinin 1 receptor; k_1 and k_2, rates of association and dissociation, respectively, of receptor; k_{rcyc}, rate of NK_1R transfer from recycling endosomes to cell surface; k_i, rate of SP-DT′ internalization; k_s, rate of SP-DT′ and NK_1R extracellular sorting; $k_{m\text{-}gm}$ and $k_{m\text{-}wm}$, rate of degradation by peptidases in gray and white matter, respectively; k_{trans}, rate of SP-DT′ transfer from endosome to cytosol; B_{max}, NK_1R capacity. *Based on fits to a kinetic model (45). †Tissue-averaged basis. ‡Approximated values.

Cytotoxic response. Approximate contours of cytotoxicity were predicted by locating the tissue regions where NK_1R-expressing cells contained ≥10 molecules of the diphtheria toxin moiety in the cytosol. This threshold number exceeds the single-molecule value reported by Yamaizumi et al. (55) as sufficient for a diphtheria toxin fragment A to kill a cell. However, this threshold is consistent with the number of molecules required to fully deplete the elongation factor 2 (EF2) pool when the fragment's half-life is taken as 16 h (47), rather than several days, as reported earlier (33, 56). {The number of toxin molecules required for depletion of the EF2 pool [$N(t)$] was computed from a model of the following form: $d[EF2]/dt = -kN(t)[EF2]$, where N and [EF2] are the number of toxin and EF2 molecules per cell, N decays exponentially from its initial loading value N_0 with a 16-h half-life, $EF2(0) \approx 2.1 \times 10^6$ molecules/cell (56), and $k = 0.001$ min^{-1}, corresponding to a toxin destruction rate of 2,000 EF2 molecules per toxin molecule per cell per minute (33). N_0 is the minimal value allowing [EF2] < 1 as $t \rightarrow \infty$.} The threshold cytosolic concentration for a neuron was thus 10 toxin molecules per neuronal cell volume of 10.8 pl (37) or 1.5 pM. Because spinal cord distributions were computed on a tissue-averaged basis and because this threshold is approached only in SP receptor-bearing neurons, 1.5 pM was converted to a tissue-averaged threshold value ($C_{cyt\ thres}$) according to $C_{cyt\ thres}$ = 1.5 pM × (fraction neuronal volume) × (fraction of NK_1R-positive neurons). The fractional neuronal volume is ~0.17 (31); the fraction of NK_1R-positive neurons varies by lamina, with the assumption of the following values: 0.45, 0.29, and 0.18 in laminae I, IV-VI, and X and 0.11 in lamina II/III (49). For lamina I, the primary drug target, $C_{cyt\ thres}$ = 0.12 pM. Lower values apply to the other laminae in accordance with their reduced NK_1R expression, but the cytotoxic contours computed for these laminae differ little from those computed using the 0.12 pM lamina I threshold because of the leading-edge steepness of the C_{cyt} concentration profiles.

Implementing the finite-element method. The equations were solved by a Galerkin finite-element method (FIDAP version 8.60, Fluent, Lebanon, NH) using an iterative segregated approach. Transient solutions were calculated with an implicit time integration scheme (2nd-order trapezoid rule) in conjunction with an adaptive time-stepping methodology. The spinal cord model was discretized into finite elements with the use of eight nodal hexahedral elements. The final mesh for the full three-dimensional model consisted of 1.5×10^6 elements. (Meshes with alternate infusion sites had similar element counts.) With consideration that the steady-state velocity field was quickly established and that the presence of infusate solute did not affect the fluid flow solution, a weakly coupled problem was assumed. Thus the solution for the steady-state velocity and pressure (*Eqs. 1* and *2*) was obtained, first, using the full three-dimensional geometry (Δz = 20.0 mm). Concentration distributions of the nonfluid components were then computed from their mass balances (*Eqs. 3–10*) while the fluid velocity values were fixed at their steady-state values. Because of prohibitively long calculation times required for the 1.5×10^6 element mesh, concentrations were determined using a truncated mesh representing a thin transverse section at the site of infusion (Δz = 0.1 mm, 65,000 elements), at which level maximum penetration of SP-DT′ occurs.

The convergence criterion for velocity and pressure was 10^{-7}, and the concentration convergence criterion was 10^{-6}.

Reduction of these criteria by two orders of magnitude did not affect results (negligible change). Mesh independence was assessed by increasing the number of elements by 30%. The resulting changes in C_{cyt} distribution after 2 and 8 h of SP-DT′ infusion were negligible. Computations were conducted on a personal computer workstation (Dell Precision 620) with dual Pentium III 1.0-GHz processors and 2.0 GB of random access memory. For calculation of an 8-h infusion, ~16 h were required for steady-state velocity and pressure simulations and ~32 h for albumin transport simulations.

RESULTS

Interstitial fluid flow field. Consistent with a previous simulation study of the rat spinal cord conducted at the same volumetric flow rate of 0.1 μl/min (44), interstitial fluid flow within the human spinal cord was predicted to be greatest in the white matter in the craniocaudal direction, parallel with the aligned fibers. Fluid flow was also predicted to skew laterally toward the white matter-CSF boundary. Interstitial fluid velocity dropped rapidly with distance from the infusion site, as presented in Fig. 3, which shows the calculated u_x decreasing with increasing distance from the infusion site along an x-directed line (Fig. 4). Because of the lower tissue permeability of gray matter, the bulk fluid flow within the gray matter regions was limited (the mean volume-averaged interstitial flow rate within a 0.1-mm-thick slice at the level of the cannula tip was calculated to be 2.5×10^{-8} cm/s in lamina I/II). To study the effect of the zero pressure boundary condition at the far end of the cord, pressure and velocity were solved for $\Delta z = 20$ and 40 mm spinal cord lengths. These interstitial velocity solutions were used to solve for the distribution of a nonreactive, nonbinding macromolecule, i.e., albumin (~66,000 mol wt). Resulting simulations showed negligible difference in craniocaudal distribution of albumin, even after 8 h of infusion at 0.1 μl/min. The computed craniocaudal distributions of albumin corresponding to 10-, 20-, and 30-μl infusions (1.7, 3.3, and 5 h) were 1.4, 1.8, and 2.2 cm, respectively

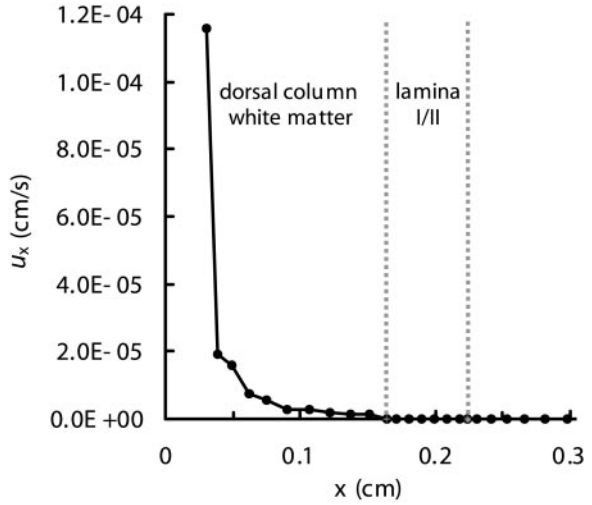

Fig. 3. Tissue-averaged velocity profile (u_x) along an x-directed line (Fig. 2) from the edge of the infusion site ($x = 0.306$ mm) and intersecting lamina I/II.

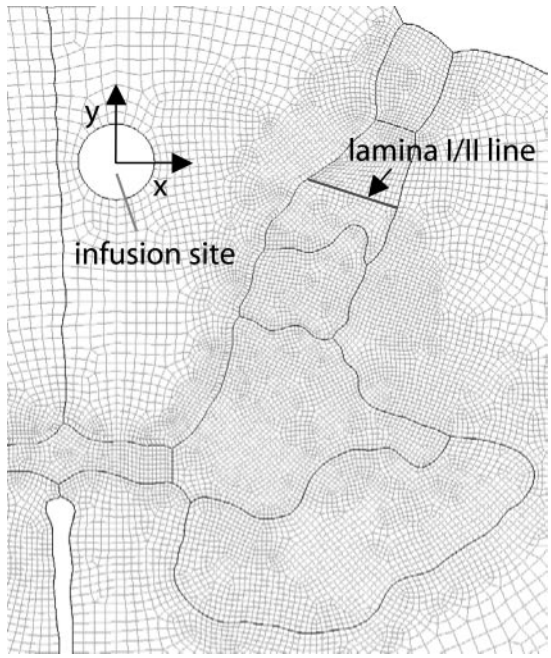

Fig. 4. Transverse section of spinal cord mesh used in finite-element calculations for transport of SP-DT′ based on projection at the C_7 level ($z = 0$). Lamina I/II line is the cross section presented in Fig. 6.

(using a $0.15\phi C_{inj}$ plotting threshold value and midline cannula placement adjacent to lamina X). When these results are compared with previous magnetic resonance imaging (MRI) measurements of gadolinium-labeled albumin infused into the lateral column of primates (26), simulation results correspond well to MRI measures for infusions up to ~4.2 h (25 μl or ~1.6 cm of craniocaudal spread).

Extracellular SP-DT′. With initial infusion, extracellular SP-DT′ was transported through the white matter interstitium by bulk flow while subject to relatively low enzymatic degradation, allowing large regions of the dorsal column to be exposed. The extracellular spread of SP-DT′ in the transverse plane containing the cannula tip during 12 h of continuous infusion of 385 nM is presented in Fig. 5, where contours are drawn at SP-DT′ concentrations that are 15% of the tissue concentration immediately adjacent to the cannula tip (i.e., $0.15\phi C_{inj}$ plotting threshold). At the times shown, SP_e is confined primarily to the white matter interstitium, and asymmetry in the distribution was due to the off-center infusion site. The extent of white matter spread depended on the level of peptidase activity. For very little activity, equivalent to the degradation rate in the CSF (23), the entire extracellular space of the dorsal column at the level of the cannula tip was filled after 12 h of infusion of 385 nM SP-DT′ at 0.1 μl/min (Fig. 5*A*). For white matter activity equal to one-half of the gray matter rate, the maximum spread did not fill the dorsal column, and spread reached an effective penetration limit after 8 h of infusion under the same conditions (Fig. 5*B*). As SP-DT′ entered the gray matter regions, it was subject to receptor uptake and degradation, and interstitial convective transport

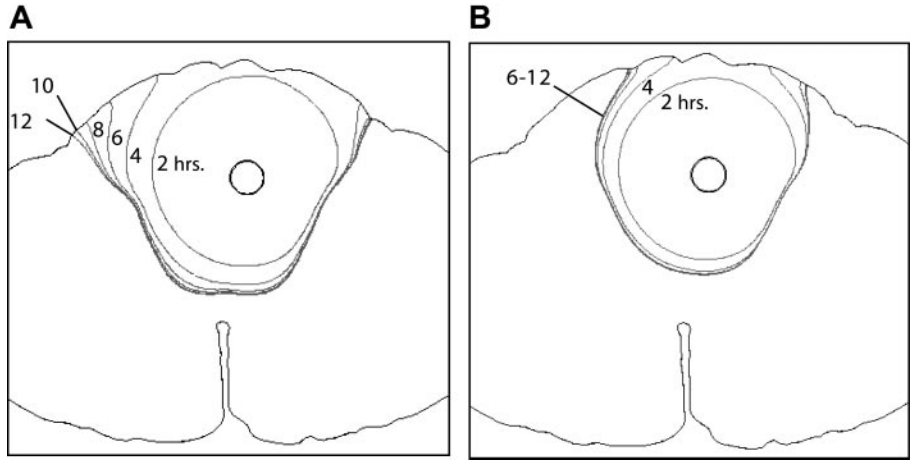

Fig. 5. Transverse spread of extracellular SP-DT′ (SP_e) over 12 h at an infusate concentration of 385 nM (z = 0). Interstitial degradation of SP-DT′ in white matter occurred at a rate equivalent to that in cerebrospinal fluid [*A*; ($k_{m\text{-}wm}$) = 0.000052 min^{-1}] or at a rate equal to one-half that in gray matter (*B*; $k_{m\text{-}wm}$ = 0.00578 min^{-1}). Contours describe location over time of SP_e concentration equal to 15% of concentration at infusion site (0.15ϕC_{inj}, where ϕ is interstitial volume fraction and C_{inj} is infusate concentration).

was greatly reduced. An SP_e concentration profile through a section of the target tissue, lamina I/II, at the level of the cannula tip is shown in Fig. 6 (8 h of infusion of 385 nM SP-DT′ at 0.1 μl/min and white matter peptidase activity of Fig. 5*A*). Here, SP_e dropped below the 15% plotting threshold (15 nM, tissue-averaged value) within 0.01 cm of the gray matter-white matter interface.

Intracellular SP-DT′. Simultaneously, concentrations of B, R, SP_s, R_s, and R_{post} within NK_1R-expressing neurons were also determined, and the cross-sectional profiles of these tissue-averaged concentrations through lamina I/II at the level of the cannula tip are presented in Fig. 6 after 8 h of infusion of 385 nM SP-DT′ at 0.1 μl/min. As SP-DT′ (SP_e) enters the laminar region, it binds strongly to cell surface NK_1Rs, first to those initially present on the cell surface and then just to those recycled to the surface. This eventually allows the rate of NK_1R internalization to balance the recycling rate over the first 0.035 cm from the gray matter-white matter interface, leading to the steady concentrations of surface-bound and endosome-borne NK_1R pools (B, R_s, and R_{post}), as well as SP_s (Fig. 6). Exposed NK_1R-expressing neurons extend through nearly 60% of the target lamina I/II at the level of the cannula tip. In unexposed regions, B, SP_s, R_s, and R_{post} are zero, and the concentration of free receptors on the cell surface (R) equals B_{max}. Cytosol concentrations of SP-DT′ were also tracked. Because of the low endosomal escape rate (k_{trans}), these concentrations were orders of magnitude smaller than those of the other cellular compartments (Fig. 7). Higher concentrations of C_{cyt} in lamina I/II and X tissue reflect the higher NK_1R densities and, thus, greater cellular uptake in these regions.

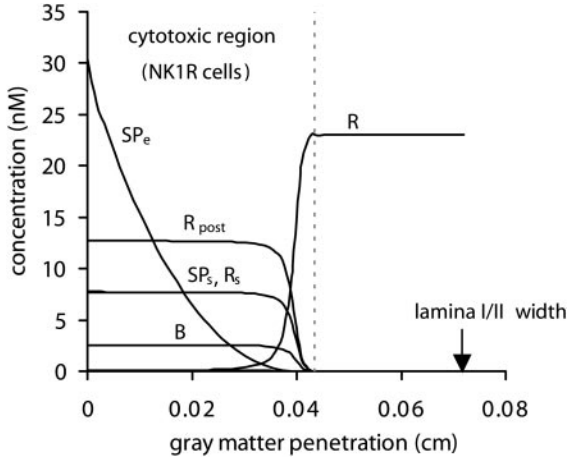

Fig. 6. Concentration profiles of SP_e, free neurokinin type 1 receptor (NK_1R) on cell surface (R), bound SP-DT′ on cell surface (B), early/sorting endosomal SP-DT′ (SP_s), early/sorting endosomal NK_1R (R_s), and NK_1R in recycling endosomes (R_{post}) after 8 h of 385 nM SP-DT′ infusion ($k_{m\text{-}wm}$ = 0.000052 min^{-1}). Concentrations are tissue-averaged values across lamina I/II (closest to infusion site at the level of infusion; see Fig. 4). Gray matter penetration equals distance from the gray matter-white matter border. Cytotoxic region is based on a threshold SP-DT′ in cytosol ($C_{cyt\,thres}$) value of 0.12 pM.

Cytotoxic regions. A cytosolic toxicity threshold of 0.12 pM was applied to predict spinal cord regions in which NK_1R-expressing neurons would be selectively ablated. The advancement of these cytotoxic regions in the transverse plane of the infusion source is presented in Fig. 8. Unless otherwise noted, the interstitial white matter degradation rate of SP-DT′ in these simulations was set equal to the CSF degradation rate (23). The initial phase of infusion caused SP-DT′ to traverse the intermediate white matter regions, and continued infusion allowed SP-DT′ to penetrate farther into the

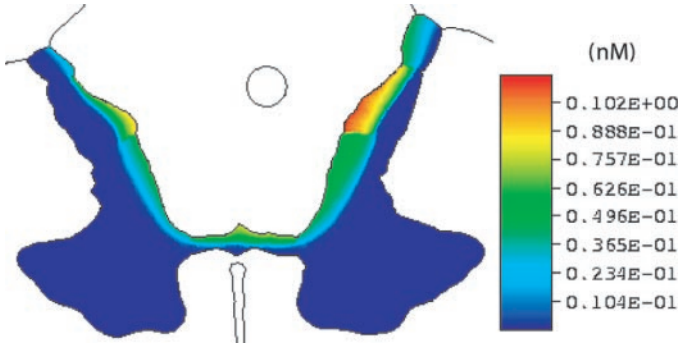

Fig. 7. Transverse concentration contour of C_{cyt} (at the level of the cannula tip) after 8 h of 385 nM SP-DT′ infusion (48-μl total infusion, $k_{m\text{-}wm}$ = 0.000052 min^{-1}). Contours are in terms of volume-averaged concentration units (nM).

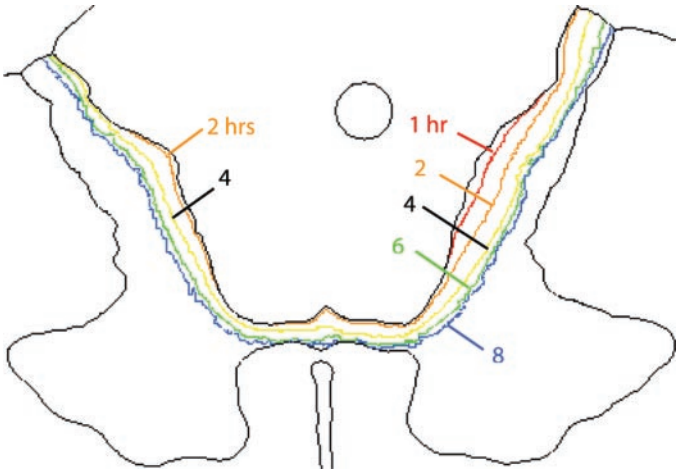

Fig. 8. Regions of cytotoxicity through a transverse section at the level of the infusion site, with infusion of 385 nM SP-DT′ for up to 8 h ($k_{m\text{-}wm}$ = 0.000052 min^{-1}). Lines correspond to cytotoxic border for 1- and 2-h intervals. Cytotoxicity was based on $C_{cyt\,thres}$ of 0.12 pM.

gray matter regions adjacent to the dorsal column. For the protocol shown in Fig. 8 (385 nM SP-DT′ with approximately central cannula placement), ~33 min (3.3 μl) of SP-DT′ infusion was required for NK_1R-expressing neurons at the nearest lamina to begin reaching cytotoxic levels. With continued infusion, cytotoxicity was predicted to extend across >60% or 0.43 mm of lamina I/II (along the cut closest to the infusion site, Figs. 4 and 6) and across the majority of the lamina X band. The predicted penetration into laminae I, II, and X, despite the presence of high concentrations of NK_1R in these regions, was not markedly different from penetration into the neighboring laminae. The rate of transverse laminar cytotoxic penetration began to slow after 6 h of infusion, and prolongation of the infusion for an additional 6 h increased the penetration by only 3% along the same lamina I/II cut. Thus predicted regions of cytotoxicity reached an effective penetration limit in the transverse direction. At the level of the cannula tip, this limit was calculated to be 6–8 h (36–48 μl) for the 0.1 μl/min infusion protocols of this study. At the same time, anterior regions of the spinal cord were unaffected.

Continued SP-DT′ spread after termination of the interstitial infusion was also analyzed. At 24 h after the baseline 8-h infusion, simulations showed that cytotoxic regions in the transverse plane containing the cannula tip did not change, except in a small region of the substantia gelatinosa on the side most distant from the infusion site (not shown). With shorter infusion periods, predicted cytotoxic regions continued to expand in this same transverse plane after the end of infusion. At 24 h after a 4-h infusion, cytotoxic spread along the lamina I/II cut closest to the infusion site increased by 9% compared with the penetration distance calculated immediately after the end of infusion (Fig. 9).

Sensitivity of the cytotoxicity zones to changes in infusion protocol was also investigated (Fig. 10). The base case for these computations was cytotoxic response for an infusate concentration of 385 nM, a volumetric infusion rate of 0.1 μl/min over 8 h, degradation rate in gray matter ($k_{m\text{-}gm}$) = 0.0116 min^{-1} (half-life = 60 min), penetration rate into white matter ($k_{m\text{-}wm}$) = 0.000052 min^{-1} (half-life = 9 days), and a central cannula tip location as depicted in Fig. 8.

First, increasing or decreasing the infusate concentration from 385 nM to 77 or 770 nM SP-DT′ resulted in a corresponding nonlinear increase or decrease in transverse cytotoxic penetration (Fig. 10*A*). Increasing the concentration to 770 nM increased the penetration along the closest lamina I/II cut by 40%. Penetration to the ventral side of lamina X was also predicted, but it was not associated with significant exposure of the anterior motor regions.

Second, movement of the infusion site to locations more proximate to the target regions was predicted to have a significant effect. Placement of the cannula tip closer to lamina I/II (Δx = 0.8 mm) resulted in a 44% increase in cytotoxic penetration along the closest lamina I/II cut relative to that for the baseline infusion location (Fig. 10*B*). Furthermore, cytotoxic penetration into lamina I/II on the opposite side was reduced. After the cannula was positioned closer to lamina X (Δy = 1.6 mm), SP-DT′ was predicted to cross lamina X and reach the motor neurons in the ventral horn via the white matter of the ventral column.

Third, use of an SP analog that is resistant to peptidase action provided for a much deeper predicted penetration into the laminae than is achieved with nonstabilized SP. Peptidase activity against neuropeptides is greater in gray than in white matter and, in the case of enkephalinase, nearly undetectable in white matter by immunoautoradiography (39). Accordingly, we determined the advantage of using stabilized SP moieties by contrasting the cytotoxicity penetration depth achieved with such an analog (characteristic peptidase degradation time of 60 min in gray matter, base case) to that achieved by nearly normal SP (characteristic degradation time of 3 min), while maintaining white matter activity at the minimal level typical of degradation in the CSF (23). At the higher gray matter degradation rate, the penetration of cytotoxicity along

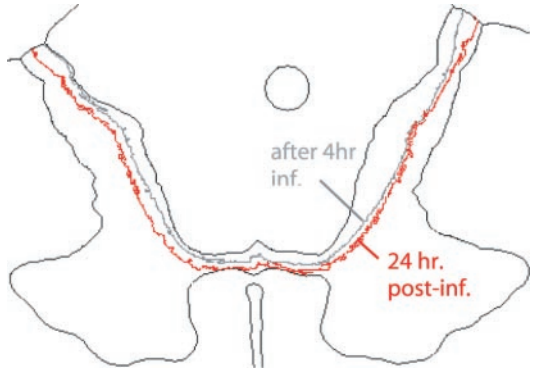

Fig. 9. Postinfusion simulation. Regions of cytotoxicity are shown in a transverse section at the level of the infusion site 24 h after a 4-h infusion of 385 nM SP-DT′ at 0.1 μl/min ($k_{m\text{-}wm}$ = 0.000052 min^{-1}). Cytotoxicity was based on $C_{cyt\,thres}$ of 0.12 pM.

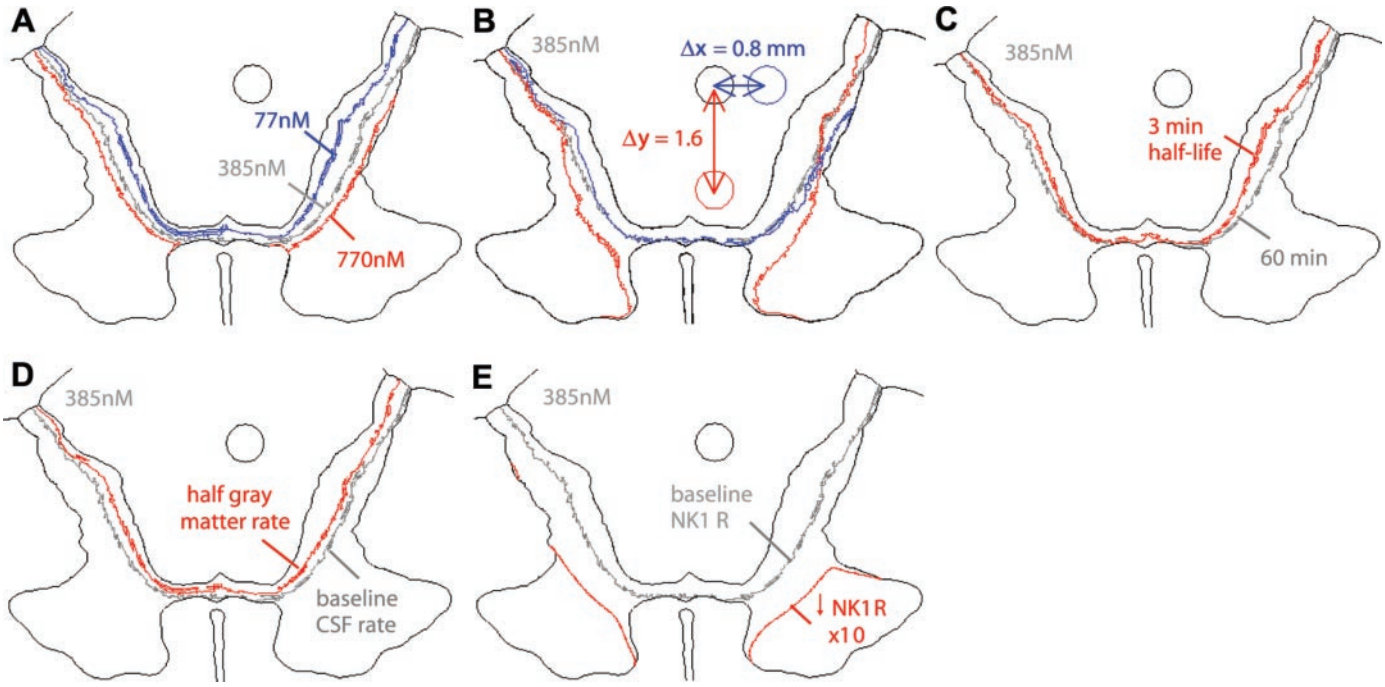

Fig. 10. Sensitivity of cytotoxic regions ($C_{cyt\,thresh}$ = 0.12 pM) in a transverse section at the level of the infusion site to changes in infusion parameters. *A*: cytotoxic contours corresponding to SP-DT′ infusate concentrations of 77, 385 (base case), and 770 nM ($k_{m\text{-}wm}$ = 0.000052 min^{-1}). *B*: cytotoxic contours corresponding to changes in infusion site location (385 nM SP-DT′ and $k_{m\text{-}wm}$ = 0.000052 min^{-1}). Gray, base case placement; blue, Δx = 0.8 mm; red, Δy = 1.6 mm. *C*: cytotoxic contours corresponding to decreasing SP analog half-life from 60 min to 3 min (385 nM SP-DT′ and $k_{m\text{-}wm}$ = 0.000052 min^{-1}). *D*: cytotoxic contours corresponding to decreasing white matter peptidase degradation rate from cerebrospinal fluid value (385 nM SP-DT′ and $k_{m\text{-}wm}$ = 0.000052 min^{-1}) to one-half that of gray matter (385 nM SP-DT′ and $k_{m\text{-}wm}$ = 0.00578 min^{-1}). *E*: cytotoxic contours corresponding to decreasing NK_1R density in gray matter from base case value (see Table 2) by a factor of 10 (385 nM SP-DT′ and $k_{m\text{-}wm}$ = 0.000052 min^{-1}). For *A*–*E*, SP-DT′ was infused for 8 h at 0.1 μl/min.

the lamina I/II cut closest to the cannula tip was predicted to decrease by 40% (Fig. 10*C*). Because peptidases other than enkephalinase are known to be active against SP in spinal cord slices (11), the possibility exists that white matter activity may be higher than the CSF activity used in our base case. A second simulation was thus performed to determine the effect of white matter peptidase activity on the extent of cytotoxicity. White matter activity was taken at an estimated upper-bound limit of one-half of the gray matter activity against the analog compound (Fig. 10*D*). With this large increase in the white matter activity (characteristic degradation time of 120 min relative to the base case time of 9 days), the extent of cytotoxicity along the lamina I/II cut closest to the cannula tip decreased by only 28%. The primary peptidase activity controlling the spread of SP analog-mediated toxicity into the laminae thus appears to be that of the gray matter.

Fourth, order-of-magnitude changes of base case laminar NK_1R densities (B_{max}) significantly affected the expected cytotoxicity distribution in the spinal cord. Although these density parameters have been well measured by autoradiography for normal and altered lumbar spinal cord after chronic constriction injury of the sciatic nerve (1), other reports indicate that binding capacities may be a fewfold different at other spinal cord levels (10), during polyarthritis (27), or after hindpaw inflammation or sciatic denervation (2). Raising the receptor concentrations throughout the laminae is predicted to be similar in effect to a decrease of infusate concentration. Hence, a fivefold increase in NK_1R would decrease the base case cytotoxic region by a degree similar to the 385 nM to 77 nM shift seen in Fig. 10*A*. On the other hand, a 10-fold decrease in NK_1R density is sufficient to shift the cytotoxic contour from its baseline position to a location well inside the ventral horn, where motor neurons would be at risk (Fig. 10*E*). During nociception, NK_1R levels have been observed to increase approximately twofold (6, 30). We have estimated that this would lead to an ~20% decrease in dorsal column penetration distance. In contrast, order-of-magnitude changes in the affinity constant [associated with peripheral inflammation or chronic constriction injury (1, 46)] were calculated to have little effect on the extent of cytotoxicity due to tight binding and the existence of a sharp moving boundary at the leading edge of the region.

DISCUSSION

By direct infusion into the white matter dorsal column of the spinal cord, large-scale, controlled distribution of macromolecular drugs along the craniocaudal

length of the spinal cord can be achieved (26, 44, 54). Corresponding transverse transport from the white matter into the adjacent gray matter is more limited. However, it may provide an ideal configuration for SP-DT′ infusion because the target neurons within laminae I, II, and X are adjacent to the white matter interface, and SP-DT′ must penetrate significant distances of interstitial gray matter before reaching NK_1R-expressing anterior motor neurons. To characterize this proposed treatment protocol, a finite-element model of SP-DT′ infusion was developed that combined mass transport, intracellular trafficking, and dose-response relations to predict the extent of transverse cytotoxicity in the spinal cord and assess whether the drug was delivered sufficiently well to kill the sensory neurons in the spinal cord that are responsible for the transmission of nociceptive signals.

For the base case simulation parameters, cytotoxic contours predict selective ablation of over one-half of the target neurons in laminae I and II at the level of the cannula tip after 8 h of 385 nM SP-DT′ infusion at 0.1 μl/min. Continually increasing regions of ablation of the target neurons were predicted with increasing infusate concentration. However, at the highest doses considered (770 nM), nonspecific binding, which is not accounted for in the present model, may occur, resulting in nonspecific damage (29, 52). In previous rat studies by Wiley and Lappi (52), intrastriatal injection of SP-saporin at high doses (~570 nM) produced regions of central necrosis at the point of injection. Similar necrosis is expected with sufficiently high doses of diphtheria toxin.

In the gray matter, a slow SP interstitial degradation rate, consistent with the in vivo degradation rate of the analog DiMeC7 (14), was considered. Such stabilized SP analog conjugates were predicted to penetrate target laminae ~60% farther than the penetration distances of more rapidly degraded native SP conjugates. Thus SP analogs stabilized against peptidase activity are expected to require a lower dose to be equally as effective as native SP conjugates. This is consistent with the observations of Wiley and Lappi (53) and Martin and Sloviter (29), who reported that relatively low doses of the [Sar^9,$Met(O_2)^{11}$]-SP conjugate, injected into the rat striatum and hippocampus, achieved tissue ablation with negligible nonspecific damage. These findings highlight the limitations of native SP as a targeting moiety and underscore the need for a degradation-resistant SP analog that reduces the likelihood of nonspecific neuronal loss by lowering the administered dose requirement.

For the degradation-resistant SP analogs considered in our simulations, transverse gray matter penetration of SP-DT′ was limited by the high binding affinity, i.e., the binding site barrier (21). Evidence of this dynamic was the great sensitivity of cytotoxic spread to NK_1R density in tissue. Thus cytotoxic spread may change according to the NK_1R distribution, which may vary with spinal cord level (10) or source and duration of pain (2, 27). Transverse cytotoxic spread was also sensitive to cannula placement. By moving the infusion site closer to the target lamina I/II, an asymmetric but more targeted ablation was achieved. Lateralized effects are desirable in all cases where nerve injury or damage affects only one limb. If bilateral treatment is required, the asymmetry in cytotoxic spread suggests that dual infusion from a symmetrically placed cannula adjacent to the corresponding lamina I/II may increase the ablation efficiency. However, care should be taken in cannula placement, inasmuch as more anterior cannula placement resulted in an increased likelihood of exposing motor neurons to the neurotoxin.

After the end of infusion, the SP-DT′ remaining in the interstitial space continues to diffuse until it is bound/internalized or degraded by peptidase action. Thus transverse cytotoxic spread was predicted to extend beyond the contours calculated immediately after the end of infusion, at least for shorter infusion times (<6–8 h at 0.1 μl/min base case). After longer infusions (>8 h), the remaining interstitial SP-DT′ cannot penetrate beyond an effective transverse penetration limit, which is determined by the balance of binding and peptidase degradation. As a result, computational analysis of the postinfusional transverse cytotoxic spread may not be necessary after longer infusions.

To be as effective as surgical procedures currently used to alleviate chronic pain, the protein toxin must also spread in the craniocaudal direction to spinal cord regions that are contacted by ascending and descending branches of primary afferent nociceptive neurons (50). Preliminary studies were conducted assessing the ability of the spinal cord model to predict interstitial transport of albumin in the craniocaudal direction. Simulation results corresponded to MRI measures for infusions up to ~25 μl. This finding corresponds with a previous porous media model of CED in the rat spinal cord (44), which shows a tendency to underestimate craniocaudal transport at larger infusion volumes. Both models predict loss of infusate solute into the adjacent CSF, suggesting that there may be an additional transport factor affecting the interstitial convective flow patterns. The pial membrane adherent to the exterior of the spinal cord may act as a fluid transport barrier, reducing the loss of fluid into the CSF. Alternatively, hydraulic conductivity may vary spatially within the white matter, with more localized deformation parallel to the white matter fibers near the infusion site. However, such transport effects are expected to have little effect on the convective flow patterns near the cannula tip and the present transverse transport analysis.

Craniocaudal cytotoxic distribution was calculated for a 25-μl infusion of SP-DT′ for a simplified case (assuming symmetry about the medial axis, i.e., the dorsal medial fissure, and central cannula placement, 2.1 mm posterior to lamina X). Simulations measuring the craniocaudal length along which there is cytotoxic penetration into lamina I/II predicted distances of 0.51, 1.36, and 1.43 cm corresponding to 10-, 20-, and 25-μl infusions of 385 nM SP-DT′ at 0.1 μl/min ($k_{m\text{-}wm}$ = 0.000052 min^{-1}). At 24 h after the end of the 25-μl infusion, the craniocaudal length along which there is

cytotoxic penetration into lamina I/II was predicted to increase by 34% over that immediately at the end of the infusion to a maximum distance of 1.9 cm. These results suggest that SP-DT′ can achieve the rostrocaudal extent necessary for treatment of chronic pain conditions that extend over one or two spinal cord segments.

The hydraulic conductivity anisotropy ratio $\kappa_{wm\text{-}z}/\kappa_{wm\text{-}x}$, determined in a previous study (44), allows prediction of the interstitial fluid flow patterns within the white matter of the spinal cord, provided infusion is limited to a volumetric flow regimen close to 0.1 μl/min. At other flow rates, the anisotropy ratio and tissue porosity may diverge from the presented values because of tissue deformation effects. It is plausible, for example, that $\kappa_{wm\text{-}z}/\kappa_{wm\text{-}x}$ and tissue porosity values may be considerably smaller in the situation of endogenous flows in normal white matter or, conversely, that these values may increase with increasing volumetric infusion rate and be associated with increased convective transport of SP-DT′.

In the determination of cytosol concentrations, uncertainty exists as to what fraction of the residence time in the sorting endosome is available for the transfer of protein toxin to the cytosol (e.g., because of changing pH or changes in budding efficiency during endosomic maturation). Delivery of the toxin to the cytosol is effectively determined by the factor $k_{trans} \times$ (time available for release to the cytosol). The k_{trans} used in this study was not determined specifically for the SP-DT′, because its value has not been measured. We used the value for transferrin-diphtheria toxin determined by Yazdi and Murphy (57), who determined that k_{trans} depends heavily on the toxic moiety and is independent of the cell line involved. However, model simulations predict that there is no significant effect on the extent of cytotoxicity with nearly an order of magnitude uncertainty in $k_{trans} \times$ (time available for release to the cytosol), because the leading edge of the cytotoxic concentration profile of diphtheria toxin is so steep. However, there may be implications for other protein toxins. Hence, SP coupled to saporin or *Pseudomonas* exotoxin may have k_{trans} values that differ greatly from that used for diphtheria toxin, resulting in different cytotoxic contours.

Interstitial infusion of SP-DT′ directly into spinal cord tissue has not been undertaken in small or large animal models. Indeed, the results of the present study provide a guideline for future experiments. In particular, further experiments are needed to determine whether partial ablation of lamina I/II (~60%) is sufficient to effectively treat chronic pain. Additional studies measuring white matter peptidase activity, nonspecific toxicity of SP-DT′, hydraulic conductivity at higher flow rates, and k_{trans} would also be useful for further model development.

Given the complex nature of the tissue response to various infusion parameters, the computational model provides aid in assessing the design and implementation of specific therapeutic protocols. The present analysis predicts that direct infusion of SP-DT′ can be used to selectively ablate NK_1-expressing neurons in laminae I, II, and X and that anterior motor neurons are not at risk with careful consideration of cannula placement, infusate concentration, and flow rate. Findings applicable to future SP-DT′ infusion designs are as follows: *1*) Longer infusions did not necessarily translate into greater transverse spread into the regions exhibiting cytotoxic susceptibility. For the infusion conditions considered in this study, maximal laminar penetration was realized between ~6 and 8 h at 0.1 μl/min (36–48 μl). *2*) High infusate concentrations provide maximal targeted ablation. However, nonspecific binding at very high concentrations should be avoided. *3*) SP analogs designed to be resistant to enzymatic degradation are required, because naturally occurring SP degrades too rapidly. *4*) Placement of the cannula adjacent to the target lamina I/II region provides for maximum laminar penetration of that side. However, care should be used in cannula placement, because more anteromedial placement may result in anterior motor neuron exposure. *5*) Accurate measurement of NK_1R density and peptidase activity in targeted spinal cord tissue is necessary, given the sensitivity of the cytotoxicity distribution to these parameters.

More generally, the type of model developed here for the spinal cord, with its inclusion of transport anisotropy, realistic anatomy, and pharmacodynamics, may now be extended to the description of drug delivery to other tissues of the CNS. Potential pharmacological agents with distribution that may be so predicted include the neurotrophic factors and excitotoxins for treatment of neurodegenerative disorders, enzymes for deficiency syndromes, genetic vectors, and radioimmunoconjugates for treatment or imaging.

The authors thank Dr. Peter Bungay for critical review of the manuscript, Drs. Rupak Banerjee, Edward Oldfield, John Heiss, and Ryszard Pluta for scientific advice, and Dr. Marc Horner and Sivaraj Sivaramakrishnan for finite-element software support.

REFERENCES

1. **Aanonsen LM, Kajander KC, Bennet GJ, and Seybold VS.** Autoradiographic analysis of ^{125}I-substance P binding in rat spinal cord following chronic constriction injury of the sciatic nerve. *Brain Res* 595: 259–268, 1992.
2. **Abbadie C, Brown JL, Mantyh PW, and Basbaum AI.** Spinal cord substance P receptor immunoreactivity increases in both inflammatory and nerve injury models of persistent pain. *Neuroscience* 70: 201–209, 1996.
3. **Barry SI and Aldis GK.** Flow-induced deformation from pressurized cavities in absorbing porous tissues. *Bull Math Biol* 54: 977–998, 1992.
4. **Basser PJ.** Interstitial pressure, volume, and flow during infusion into brain tissue. *Microvasc Res* 44: 143–165, 1992.
5. **Benoliel R, Eliav E, Mannes AJ, Caudle RM, Leeman S, and Iadarola MJ.** Actions of intrathecal diphtheria toxin-substance P fusion protein on models of persistent pain. *Pain* 79: 243–253, 1999.
6. **Benoliel R, Tanaka M, Caudle RM, and Iadarola MJ.** Colocalization of *N*-methyl-D-aspartate receptors and substance P (neurokinin-1) receptors in rat spinal cord. *Neurosci Lett* 291: 61–64, 2000.
7. **Bobo RH, Laske DW, Akbasak A, Morrison PF, Dedrick RL, and Oldfield EH.** Convection-enhanced delivery of macromolecules in the brain. *Proc Natl Acad Sci USA* 91: 2076–2080, 1994.

8. **Bowden JJ, Garland AM, Baluk P, Lefevre P, Grady EF, Vigna SR, Bunnet NW, and McDonald DM.** Direct observation of substance P-induced internalization of neurokinin 1 (NK_1) receptors at sites of inflammation. *Proc Natl Acad Sci USA* 91: 8964–8968, 1994.
9. **Bradbury M.** *The Concept of a Blood-Brain Barrier*. New York: Wiley, 1979.
10. **Charlton CG and Helke CJ.** Characterization and segmental distribution of ^{125}I-Bolton-Hunter-labeled substance P binding sites in rat spinal cord. *J Neurosci* 5: 1293–1299, 1985.
11. **Chen JJ, Barber LA, Dymshitz J, and Vasko MR.** Peptidase inhibitors improve recovery of substance P and calcitonin gene-related peptide release from rat spinal cord slices. *Peptides* 17: 31–37, 1996.
12. **Chen MY, Lonser RR, Morrison PF, Governale LS, and Oldfield EH.** Variables affecting convection-enhanced delivery to the striatum: a systematic examination of rate of infusion, cannula size, infusate concentration, and tissue-cannula sealing time. *J Neurosurg* 90: 315–320, 1999.
13. **Croul S, Radzievsky A, Sverstiuk A, and Murray M.** NK_1, NMDA, $5HT_{1a}$, and $5HT_2$ receptor binding sites in the rat lumbar spinal cord: modulation following sciatic nerve crush. *Exp Neurol* 154: 66–79, 1998.
14. **Eison AS, Iversen SD, Sandberg BEB, Watson SP, Hanley MR, and Iversen LL.** Substance P analog, DiMe-C7: evidence for stability in rat brain and prolonged central actions. *Science* 215: 188–190, 1982.
15. **Fisher CE, Sutherland JA, Krause JE, Murphy JR, Leeman SE, and VanderSpek JC.** Genetic construction and properties of diphtheria toxin-related substance P receptors. *Proc Natl Acad Sci USA* 93: 7341–7345, 1996.
16. **Garland AM, Grady EF, Payan DG, Vigna SR, and Bunnett NW.** Agonist-induced internalization of the substance P (NK_1) receptor expressed in epithelial cells. *Biochem J* 303: 177–186, 1994.
17. **Geppetti P, Santicioli P, Rubini I, Spillantini MG, Maggi CA, and Sicuteri F.** Thiorphan increases capsaicin-evoked release of substance P from slices of dorsal spinal cord of guinea pig. *Neurosci Lett* 103: 69–73, 1989.
18. **Grady EF, Garland AM, Gamp PD, Lovett M, Payan DG, and Bunnett NW.** Delineation of the endocytic pathway of substance P and its seven-transmembrane domain NK_1 receptor. *Mol Biol Cell* 6: 509–524, 1995.
19. **Haines DE.** *Neuroanatomy: An Atlas of Structures, Sections, and Systems* (4th ed.). Baltimore, MD: Williams & Wilkins, 1995.
20. **Hausman L.** *Photographs of Microscopic Serial Sections of the Human Spinal Cord and Brain: Photographic Supplement to Atlas I*. Springfield, IL: Thomas, 1969.
21. **Juweid M, Neumann R, Paik C, Perez-Bacete J, Sato J, van Osdol WW, and Weinstein JN.** Micropharmacology of monoclonal antibodies in solid tumors: direct experimental evidence for a binding site barrier. *Cancer Res* 54: 5144–5153, 1992.
22. **Kalyanasundaram V, Calhoun VD, and Leong KW.** A finite element model for predicting the distribution of drugs delivered intracranially to the brain. *Am J Physiol Regul Integr Comp Physiol* 273: R1810–R1821, 1997.
23. **Kaneko T, Wood G, Crouch WL, and Desiderio DM.** Substance P-inactivating enzymes in human cerebrospinal fluid. *Peptides* 15: 41–47, 1994.
24. **Laske DW, Morrison PF, Lieberman DM, Corthesy ME, Reynolds JC, Stewart Henney PA, Koong SS, Cummins A, Paik CH, and Oldfield EH.** Chronic interstitial infusion of protein to primate brain: determination of drug distribution and clearance with single-photon emission computerized tomography imaging. *J Neurosurg* 87: 586–594, 1997.
25. **Lieberman DM, Laske DW, Morrison PF, Bankiewicz KS, and Oldfield ED.** Convection-enhanced distribution of large molecules in gray matter during interstitial drug infusion. *J Neurosurg* 82: 1021–1029, 1995.
26. **Lonser RR, Gogate N, Morrison PF, Wood JD, and Oldfield EH.** Direct convective delivery of macromolecules to the spinal cord. *J Neurosurg* 89: 610–615, 1998.
27. **Mantyh CR, Gates T, Zimmerman RP, Kruger L, Maggio JE, Vigna SR, Basbaum AI, Levine J, and Mantyh PW.** Alterations in the density of receptor binding sites for sensory neuropeptides in the spinal cord of arthritic rats. In: *The Arthritic Rat as a Model of Clinical Pain?*, edited by Besson JM and Guilbaud G. Amsterdam: Excerpta Medica, 1988, p. 139–152.
28. **Mantyh PW, Rogers SD, Honore P, Allen BJ, Ghilardi JR, Li J, Basbaum AI, Daughters RS, Lappi DA, Wiley RG, and Simone DA.** Inhibition of hyperalgesia by ablation of lamina I spinal neurons expressing the substance P receptor. *Science* 278: 275–283, 1997.
29. **Martin JL and Sloviter RS.** Focal inhibitory interneuron loss and principal cell hyperexcitability in the rat hippocampus after microinjection of a neurotoxic conjugate of saporin and a peptidase-resistant analog of substance P. *J Comp Neurol* 436: 127–152, 2001.
30. **McCarson KE and Krause JE.** NK-1 and NK-3 type tachykinin receptor mRNA expression in the rat spinal cord dorsal horn is increased during adjuvant- or formalin-induced nociception. *J Neurosci* 14: 712–720, 1994.
31. **Mooney SM, Napper RMA, and West JR.** Long-term effect of postnatal alcohol exposure on the number of cells in the neocortex of the rat: a stereological study. *Alcohol Clin Exp Res* 20: 615–623, 1996.
32. **Morrison PF, Laske DW, Bobo H, Oldfield EH, and Dedrick RL.** High-flow microinfusion: tissue penetration and pharmacodynamics. *Am J Physiol Regul Integr Comp Physiol* 266: R292–R305, 1994.
33. **Moynihan MR and Pappenheimer AM.** Kinetics of adenosine diphosphoribosylation of elongation factor-II in cells exposed to diphtheria toxin. *Infect Immun* 32: 575–582, 1981.
34. **Nagashima T, Shirakuni T, and Rapoport SI.** A two-dimensional, finite element analysis of vasogenic brain edema. *Neurol Med Chir (Tokyo)* 30: 1–9, 1990.
35. **Nichols ML, Allen BJ, Rogers SD, Ghilardi JR, Honore P, Luger NM, Finke MP, Li J, Lappi DA, Simone DA, and Mantyh PW.** Transmission of chronic nociception by spinal neurons expressing the substance P receptor. *Science* 286: 1558–1561, 1999.
36. **Nicholson C and Sykova E.** Extracellular space structure revealed by diffusion analysis. *Trends Neurosci* 21: 207–215, 1998.
37. **Pannese E, Barni L, Arcidiacono G, and Ledda M.** Cell body volume of spinal ganglion neurons: estimation by three different methods. *J Submicrosc Cytol Pathol* 29: 497–502, 1997.
38. **Paxinos G.** *The Rat Brain in Stereotaxic Coordinates* (2nd ed.). New York: Academic, 1986.
39. **Pollard H, Bouthenet ML, Moreau J, Souil E, Verroust P, Ronco P, and Schwartz JC.** Detailed immunoautoradiographic mapping of enkephalinase (EC 3.42411) in rat central nervous system—comparison with enkephalins and substance P. *Neuroscience* 30: 339–376, 1989.
40. **Prabhu SS, Broaddus WC, Gillies GT, Loudon WG, Chen Z, and Smith B.** Distribution of macromolecular dyes in brain using positive-pressure infusion: a model for direct controlled delivery of therapeutic agents. *Surg Neurol* 50: 367–375, 1998.
41. **Prokopova S, Vargova L, and Sykova E.** Heterogeneous and anisotropic diffusion in the developing rat spinal cord. *Neuroreport* 8: 3527–3532, 1997.
42. **Reulen HJ, Graham R, Spatz M, and Klatzo I.** Role of pressure gradients and bulk flow in dynamics of vasogenic brain edema. *J Neurosurg* 46: 24–35, 1977.
43. **Saltzman WM and Radomsky ML.** Drugs released from polymers: diffusion and elimination in brain tissue. *Chem Eng Sci* 46: 2429–2444, 1991.
44. **Sarntinoranont M, Banerjee Lonser RR, and Morrison PF.** A computational model of direct interstitial infusion of macromolecules into the spinal cord. *Ann Biomed Eng* 31: 448–461, 2003.
45. **Sarntinoranont M, Iadarola MJ, and Morrison PF.** A kinetic analysis of substance P trafficking. *J Pharm Sci* 92: 232–243, 2003.
46. **Stucky CL, Galeazza MT, and Seybold VS.** Time-dependent changes in Bolton-Hunter-labeled ^{125}I-substance P binding in

rat spinal cord following unilateral adjuvant-induced peripheral inflammation. *Neuroscience* 57: 397–409, 1993.
47. **Sung C, Wilson D, and Youle RJ.** Comparison of protein synthesis inhibition kinetics and cell killing induced by immunotoxins. *J Biol Chem* 266: 14159–14162, 1991.
48. **Tao L and Nicholson C.** Diffusion of albumins in rat cortical slices and relevance to volume transmission. *Neuroscience* 75: 839–847, 1996.
49. **Todd AJ, Spike RC, and Polgar E.** A quantitative study of neurons which express neurokinin-1 or somatostatin sst(2a) receptor in rat spinal dorsal horn. *Neuroscience* 85: 459–473, 1998.
50. **Traub RJ, Iadarola MJ, and Ruda MA.** Effect of multiple dorsal rhizotomies on calcitonin gene-related peptide-like immunoreactivity in the lumbosacral dorsal spinal cord of the cat—a radioimmunoassay analysis. *Peptides* 10: 979–983, 1989.
51. **Vigna SR, Bowden JJ, McDonald DM, Fisher J, Okamoto A, McVey DC, Payan DG, and Bunnet NW.** Characterization of antibodies to the rat substance P (NK-1) receptor and to a chimeric substance P receptor expressed in mammalian cells. *J Neurosci* 14: 834–845, 1994.
52. **Wiley RG and Lappi DA.** Destruction of neurokinin-1 receptor-expressing cells in vitro and in vivo using substance P-saporin in rats. *Neurosci Lett* 230: 97–100, 1997.
53. **Wiley RG and Lappi DA.** Targeting neurokinin-1 receptor-expressing neurons with [Sar^{9},$Met(O_2)^{11}$]substance P-saporin. *Neurosci Lett* 277: 1–4, 1999.
54. **Wood JD, Lonser RR, Gogate N, Morrison PF, and Oldfield EH.** Convective delivery of macromolecules into the naive and traumatized spinal cords of rats. *J Neurosurg* 90: 115–120, 1999.
55. **Yamaizumi M, Mekada E, Uchida T, and Okada Y.** One molecule of diphtheria toxin fragment A introduced into a cell can kill the cell. *Cell* 15: 245–250, 1978.
56. **Yamaizumi M, Uchida T, Takamatsu K, and Okada Y.** Intracellular stability of diphtheria toxin fragment A in the presence and absence of anti-fragment A antibody. *Proc Natl Acad Sci USA* 79: 461–465, 1982.
57. **Yazdi PT and Murphy RM.** Quantitative analysis of protein synthesis inhibition by transferrin-toxin conjugates. *Cancer Res* 54: 6387–6394, 1994.